IPPP/01/34
DCPT/02/68
IC/HEP/01-2

SUMMARY OF THE STRUCTURE FUNCTION SESSION AT DIS01*

KENNETH LONG
Imperial College London, UK, E-mail: K.Long@ic.ac.uk

RICHARD NISIUS
CERN, Switzerland, E-mail: Richard.Nisius@cern.ch

W. JAMES STIRLING
IPPP Durham, England, E-mail: W.J.Stirling@durham.ac.uk

The status and ongoing developments in the field of deep inelastic scattering presented at the DIS01 workshop in Bologna are discussed from both the experimental and the theoretical perspective.

1 Introduction

In the last year considerable progress has been made in many aspects of the study of the structure functions of photons and nuclei. The most important results presented in the structure function session at the DIS01 workshop in Bologna are reviewed. The new theoretical developments are discussed in Section 2. New experimental information on photon structure is summarised in Section 3 while Section 4 reviews the new experimental results pertaining to the structure of the proton. The material presented here is intended only as an overview, and reflects the personal view of the working group convenors. Many of the important details of the investigations have of necessity had to be omitted. The reader is referred to the write-ups of the individual presentations that are to be found elsewhere in these proceedings.

2 Theory

It is remarkable that a theoretical framework that was established more than twenty years ago – short-distance factorisation and next-to-leading (NLO) DGLAP – still gives a very good description of almost all deep inelastic structure function data, for example see Section 4 below. In recent years attention has focused on calculations that attempt to improve the theoretical prediction by going beyond the standard 'massless quark NLO–DGLAP' framework.

*INVITED TALK PRESENTED AT THE 9TH INTERNATIONAL WORKSHOP ON DEEP INELASTIC SCATTERING (DIS 2001), BOLOGNA, ITALY, 27 APR - 1 MAY 2001, TO APPEAR IN THE PROCEEDINGS.

Previous DIS Workshops reported the significant progress on incorporating non-zero quark masses (particularly m_c) into the analysis, and the resulting improved calculations are now used routinely in the experimental analyses. The outstanding theoretical deficiencies and uncertainties can be classified into various types. Within leading-twist perturbation theory, the obvious goal is a complete NNLO description. At least for massless quarks, this seems to be within reach (see below) and the likely phenomenological impact has already been investigated. A variation of this approach is to focus on the kinematic $x \to 0,\ 1$ limits and resum the leading logarithmic corrections to all orders in perturbation theory, to investigate whether the fit to data is improved. Non-perturbative corrections arise in various ways, for example higher twist $\left(1/Q^2\right)^n,\ n \geq 1$ power corrections, and also heavy nuclear target corrections. A number of theoretical contributions to this session addressed these issues, and the main results of these studies are summarised briefly below.

Parton distribution functions (PDFs) extracted from deep inelastic scattering structure functions data play a central role in the calculation of hard scattering cross sections at the Tevatron and LHC. A precise knowledge of the PDFs is absolutely vital for reliable predictions for signal and background cross sections. In many cases, it is the uncertainty in the input PDFs that dominates the theoretical error on the prediction. Such uncertainties can arise both from the starting distributions themselves, reflecting the uncertainties in the data input to the global fit, and from evolution to the higher Q^2 scales typical of hadron collider hard scattering processes, which is sensitive to uncertainties in α_s, unknown higher-order corrections, other parton flavours, etc. By way of illustration, Figure 1 shows the (x, Q^2) values corresponding to the production of heavy objects (e.g. a W or Higgs boson, a $t\bar{t}$ pair, a multijet final state etc.) of mass M and rapidity y. We assume leading order kinematics, so that $x = M \exp(\pm y)/\sqrt{s}$ and $Q = M$. As an example, a W boson ($M = 80$ GeV) produced at rapidity $y = 3$ corresponds to the annihilation of quarks with $x = 0.00028$ and 0.11, probed at $Q^2 = 6400$ GeV^2. Notice that in this example, quarks with these x values are already 'measured' in deep inelastic scattering (at HERA and in fixed–target experiments respectively), but at much lower Q^2.

A rigorous and global treatment of *PDF uncertainties* remains elusive, but there has been a significant advance in the last few years, with several groups now introducing sophisticated statistical analyses into global or quasi-global fits. Further progress was reported at this meeting and is summarised below.

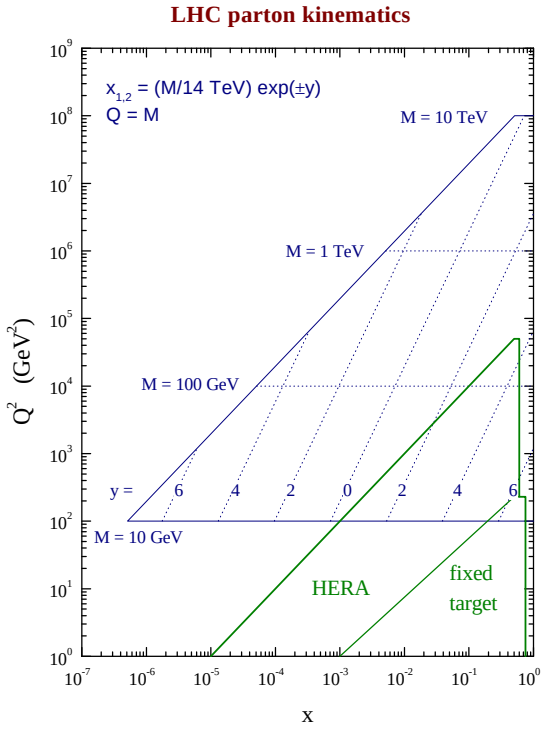

Figure 1. x and Q^2 values probed in the production of an object of mass M and rapidity y at LHC.

2.1 Higher orders, higher twists

In order to match the precision of present and future DIS data, it is necessary to go beyond NLO in DGLAP perturbation theory. The most relevant quantities here are the NNLO contribution to the DGLAP splitting functions, i.e. the functions $P^{(2)}$ in the expansion

$$\text{Splitting Function:} \qquad P(x,\alpha_s) = P^{(0)} + \alpha_s P^{(1)}(x) + \alpha_s^2 P^{(2)}(x) + ... \quad (1)$$

together with the corresponding coefficient functions:

$$\text{Coefficient Function:} \qquad \hat{\sigma} = \alpha_s^n \left[\hat{\sigma}^{(0)} + \alpha_s \hat{\sigma}^{(1)} + \alpha_s^2 \hat{\sigma}^{(2)} + ... \right] \quad (2)$$

The NNLO contributions to the latter are easier to calculate and are already known for many of the cross sections and structure functions of interest.[a]

Using recent $N = 10, 12$ moment calculations by Retey and Vermaseren[1], van Neerven and Vogt[2] have updated their approximations for $P^{(2)}(x)$, in which the moment information is combined with sum rule and symmetry constraints and known leading behaviour for $x \to 0, 1$. The resulting approximate functions are certainly sufficient for $x > 10^{-2}$ phenomenology, and probably adequate for $x > 10^{-4}$ as well. Further information can be found in the contribution by Vogt to these proceedings[3]. It was reported by Vogt at the meeting that the exact calculation of the NNLO splitting functions should be completed by the end of the year.

Fully *quantitative* predictions for higher-twist contributions to DIS structure functions remain elusive. A potentially important twist–4 contribution comes from the 4–gluon operator matrix element combined with the 4 gluon $\to$ 2 quark coefficient function. Blümlein[4] presented an estimate of this contribution to the structure function slope $\partial F_2/\partial \log Q^2$. The calculation[5] is performed using time–ordered perturbation theory and is limited to dp_T^2/p_T^4 accuracy in the calculation of the corresponding Feynman diagrams. Numerical results are obtained by modeling the $4g$ distribution amplitude. At small x it is the *screening* (rather than anti-screening) terms which dominate and reduce the increase of the slope due to the leading twist–2 contributions. The numerical results, see Figure 2, show that this effect is significant only below $x \sim 2 \cdot 10^{-6}$ for $Q^2 \sim 5$ GeV^2. This is beyond the kinematic range that can be probed at HERA but may be accessible at future lepton–hadron colliders operating at higher energies.

Another type of power correction, of more universal origin, can arise from analytic resummation of perturbative contributions to all orders. Such resummations typically lead to expressions of the form

$$f(Q^2) \propto \int_0^{Q^2} \frac{dk^2}{k^2} (k^2)^a \alpha_s(k^2) \tag{3}$$

which are ill-defined because of the Landau pole in the running coupling. Expanding $\alpha_s(k^2)$ in powers of $\alpha_s(Q^2)$ yields a perturbation series for f whose coefficients grow as $n!$. The resulting ambiguity in the resummed perturbative result signals a nonperturbative power correction of the form $(\Lambda^2/Q^2)^a$. An alternative way to tackle this problem, in the context of QCD quark form factors, using dimensional regularisation was presented by Magnea[6] (see also

[a] Note however that $\hat{\sigma}^{(2)}$ is still not calculated for some of the key cross sections used in global fits, e.g. $d\sigma/dE_T^{jet}$, $d\sigma/dy_W$, $d^2\sigma^{DY}/dM\,dy$, etc.

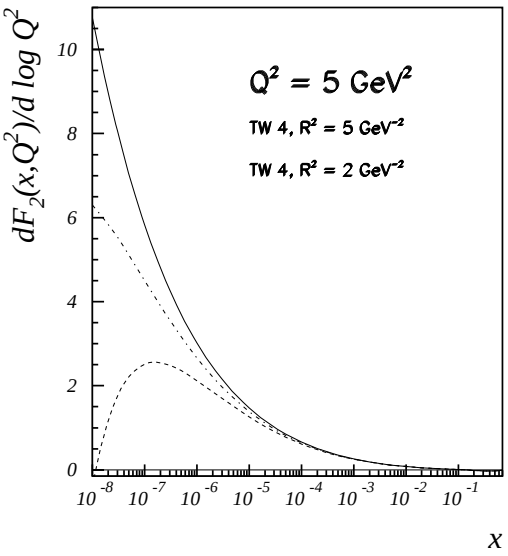

Figure 2. Contributions to the slope $\partial F_2/\partial \log Q^2$ from twist–2 (solid line) and twist–4 (dash-dotted and dotted lines) operators, with two values of the twist–4 mass scale R^2 for the latter, from the study by Blümlein *et al.*[5].

[7]). If the calculation is performed consistently in $d = 4 - 2\epsilon > 4$ dimensions then the pole moves off the real axis and analytic resummed expressions for the form factors can be obtained in terms of gauge and renormalisation-group invariant quantities. Applying these techniques to the physically relevant DIS structure function (N) moments yields the standard expression $\propto N(\Lambda^2/Q^2)$ for the leading power correction at large N. The generalisation to more complicated QCD amplitudes, for example those involving at least two coloured particles, is more difficult and more work needs to be done.

Small-x structure function phenomenology incorporating higher-twist contributions was the subject of a presentation by Kotikov[8]. The starting point of the analysis is the set of analytic solutions of the DGLAP equations at small x obtained from a flat parton input at Q_0^2 [9]. These solutions are supplemented by higher-twist (twists 4 and 6) contributions as obtained in a renormalon model[10]. A very reasonable few-parameter fit to HERA structure function data is obtained (see [8]), suggesting that higher-twist contributions do contribute to the observed rise of the F_2 structure function at low values

of x and Q^2.

Another example of QCD resummation was discussed by Ermolaev[11] in the context of the small-x asymptotics of the non-singlet unpolarised and polarised structure functions. Accounting for both double- and single-logarithmic contributions and *using a fixed QCD coupling* yields the asymptotic behaviour,

$$F_1^{NS}, g_1^{NS} \sim \left(\frac{1}{x}\sqrt{\frac{Q^2}{\mu^2}}\right)^{a_\pm} \tag{4}$$

$$a_+ = \sqrt{2\alpha_s C_F/\pi}, \qquad a_- = a_+\,\sqrt{1+1/(2N^2)} \tag{5}$$

The situation is more complicated when α_s is allowed to run with the internal ladder transverse momenta as arguments[12]. Two-dimensional infrared evolution equations are constructed and solved numerically. The exponents $a_\pm$ become functions of $\Lambda_{\rm QCD}$ and μ, the infrared cut-off parameter. Quantitatively, $a_\pm \to \omega_\pm(\mu) = 0.37/0.4$ at 1 GeV, which in fact is in good agreement with the phenomenological values extracted from fits to xF_3 data at small x.

Finally, it is by now well established that it is difficult to disentangle the underlying small-x QCD dynamics (BFKL, CCFM, DGLAP, etc.) from inclusive quantities (e.g. F_2) alone. More exclusive quantities, for example transverse energy flow and dijet production rates and correlations, offer a more decisive test, at least in principle. Szczurek[13] presented the results of a study[14] of how dijet azimuthal correlations $d\sigma/d\phi_{\rm jj}$ in real and virtual photoproduction at HERA can be used to probe the unintegrated gluon $g(x,k_\perp^2)$ in the proton. The benchmark distribution used in the study is the two-component (soft + hard) model of Ivanov and Nikolaev[15], which leads to distinctive kinematical dependence of the dijet correlations. It will be important to make comparisons with the predictions of other models, and of course with data.

2.2 PDF fits and uncertainties

Progress in obtaining an improved quantitative understanding of parton distribution functions and their uncertainties was reported at the meeting. In the context of 'best global fits', Thorne[16] reported on a recent update of the MRST (NLO–DGLAP) global fit. The main new ingredients in the fit are (a) new small-x structure function data from HERA, and (b) new high-E_T jet data from the Tevatron (see Section 4.2 below for more details). For the latter, a proper treatment of the correlations between the various systematic errors is essential and is incorporated in the MRST fitting procedure. The main effect of the new data is to further constrain the gluon distribution at both

small and large x. As for previous global analyses, the overall fit is very good, but there are some interesting new features: (i) the negativity of the small-x (NLO, $\overline{\rm MS}$) gluon near the starting scale at 1 GeV^2 is now firmly established (although the gluon becomes positive for all $x > 10^{-5}$ for $Q^2 > 2 - 3$ GeV^2); (ii) there is a slight 'tension' between the $\alpha_s(M_Z^2)$ values preferred by the DIS (0.121) and jet (0.117) data.

Turning to uncertainties on (or due to) PDFs, the MRST approach[17] (see also [18,19]) has been to focus on the uncertainties on particular physical quantities $\delta\sigma_{\rm obs}$ (for example, the Higgs or weak boson production cross sections), rather than on uncertainties on the PDFs themselves, δf_i [20,21,22,23,24]. Thorne reported on a new determination of the PDF uncertainty on σ_W at the Tevatron and LHC. A previous investigation of this uncertainty using the Lagrange Multiplier method[18] (see below) had resulted in $\delta\sigma_{\rm PDF} \simeq 5 - 8\%$. The MRST approach is to determine which parts of the global fit fail when trying to force higher/lower $\sigma_{\rm obs}$, and to impose the criterion that no individual data set has a less than 1% confidence level. This leads to an estimate of the PDF dependent uncertainty in the total W cross section of $\simeq \pm 2\%$ at both the Tevatron and LHC. An example of how one of the components of the MRST global fit fails when σ_W is forced up and down from its central prediction is shown in Figure 3.

Recent work on parton distribution uncertainties in the context of the CTEQ global fit was reviewed by Stump[25]. Two methods have been adopted. In the Lagrange Multiplier constrained fitting approach[22] the global fit is repeated for successive constrained values of a physical observable σ_X, and a $\chi^2_{\rm global}$ *vs.* σ_X profile is established. The issue is then what 'tolerance' (increase in $\chi^2_{\rm global}$ from the minimum) corresponds to a standard confidence level. In the CTEQ study, the tolerance is determined by considering the χ^2 response of the individual experiments to the sample PDFs. The 90% CL allowed ranges for each experiment are then combined into a single overall tolerance. The second 'Hessian Matrix' approach follows a more traditional error analysis by focusing on the allowed ranges of the individual parameters $a_1, ...a_d$ that define the PDFs:

$$\chi^2_{\rm global} = \chi^2_0 + \sum_{i,j=1}^{d} (a_i - a_i^0) H_{ij} (a_j - a_j^0) + \ldots \tag{6}$$

Assuming a quadratic approximation, the error on a given observable X is then

$$(\Delta X)^2 = \Delta\chi^2 \sum_{i,j} \frac{\partial X}{\partial a_i} \left(H^{-1}\right)_{ij} \frac{\partial X}{\partial a_j} \tag{7}$$

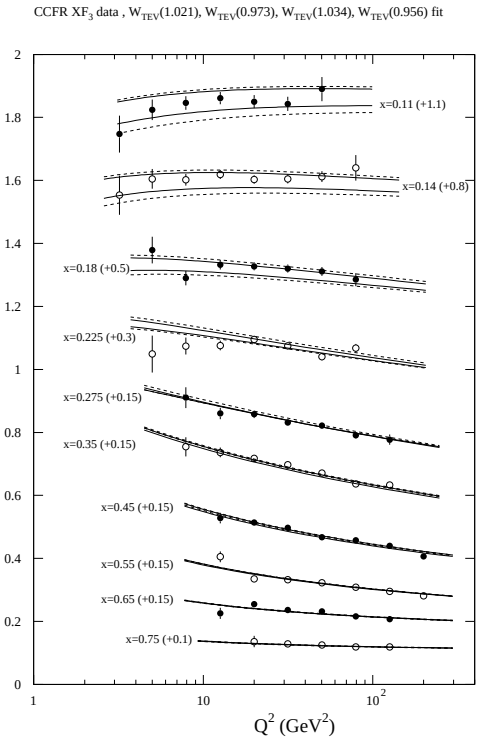

Figure 3. Comparison of CCFR $F_3(x, Q^2)$ data with theory for σ_W(TEV) changing in magnitude by factors of 1.021, 0.973, 1.034 and 0.956, from the new MRST study reported by Thorne[16].

The eigenvectors of the Hessian matrix H define orthogonal directions in parameter space that can be used to define a set of $(2d + 1)$ PDF basis sets. Again there is the issue of the definition of the standard tolerance, i.e. the allowed variation of $\Delta\chi^2$ in Equation 7. The PDF basis sets can also be used to define bands of uncertainty for individual PDFs as the envelope of the extreme curves at given values of x. An example is shown in Figure 4. Notice how the band shrinks as Q^2 increases, and also how the choice of parametric form causes a slight (artificial) decrease in the band width between the low and high x regions.

Finally, in a thought-provoking contribution Collins[26] (see also [27]) ad-

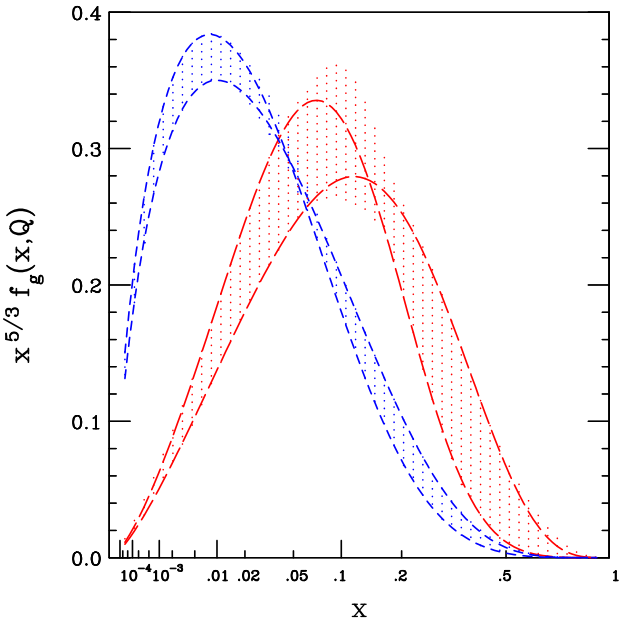

Figure 4. Extreme gluon distributions at $Q = 2$ and 10 GeV, from the CTEQ Hessian Matrix error analysis[22]. The curves show the extremes at some particular x, while the shaded regions represent the envelope of such extremes.

dressed the issue of how to determine how 'good' a good global fit really is. The point is that a reasonable overall $\chi^2_{\rm tot}$ can mask the fact that certain subsets of data (i.e. individual experiments) are in strong disagreement with the theory (which could of course have various explanations, ranging from errors or deficiencies in the experimental analysis or theoretical calculation to an unexpected contribution from new physics). The procedure is therefore to consider the quality of fit to individual data subsets, explore the parameter space to find PDF sets that are 'best fits' to these individual data sets and to examine by how much the fit to a particular data set is improved relative to the increase in overall $\chi^2_{\rm tot}$. A substantial decrease in an individual χ^2 is a symptom of a bad fit to that particular data set, which could then be further studied to investigate the source of the disagreement. It is interesting to note

that both the CTEQ and MRST global fits contain 'problem' data subsets according to this definition.

2.3 Parton distributions in heavy nuclei

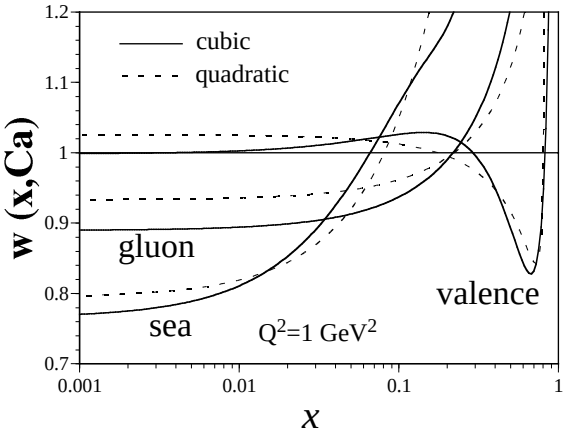

Figure 5. The weight functions of Equation 8 for parton distributions in calcium, from the study by Kumano *et al.*[29].

When deep inelastic neutrino scattering structure function data are used in a global PDF fit, account must be taken of the fact that the PDFs in heavy nuclei are *different* from those in a nucleon. It is important to quantify these differences, not only for use in global PDF fits but also, for example, when interpreting possible quark-gluon plasma signals from heavy ion collisions. There have been several recent analyses to determine the parton distributions in nuclei[28,29,30]. Kumano[28] reported the results of a study[29] based on fits to electron and muon F_2 data on nuclear targets. A simple ansatz is used to parameterise the nuclear modification of the PDFs:

$$\begin{aligned} f_i^A(x,Q^2) &= w_i(x,A)\; f_i^N(x,Q^2) \\ w_i(x,A) &= 1 + \left(1 - A^{-1}\right)^{1/3} h_i(x) \end{aligned} \tag{8}$$

where h_i is taken to be either a quadratic or cubic polynomial in x divided by a power of $(1-x)$. The parameters in h_i are determined by a χ^2 minimisation procedure. A reasonable overall fit is obtained ($\chi^2/\mathrm{dof} = 580/302$), with the excess χ^2 mainly due to apparent inconsistencies between data sets, e.g. E665

vs. NMC. The resulting weight functions for calcium are shown in Figure 5. As only structure function data are used in the fit, there are large uncertainties on the extracted gluon and sea-quark weight functions. Comparisons with Drell-Yan, prompt-γ and heavy quark production data are needed to further constrain g^A, $\bar{q}^A$, see for example[31,32].

3 Photon Structure

The investigation of the structure of the photon is a very active field of research at LEP as well as at HERA, see[33] for a recent review. At this conference new results from LEP and HERA have been presented which are briefly summarised here.

New investigations on the structure of the photon based on jet production were presented by H1 for quasi-real[34], and by ZEUS for virtual[35] photons. The new H1 result, Figure 6, is consistent with the predictions based on existing parametrisations of the hadronic photon structure function F_2^γ and at present the data are not precise enough to distinguish between different parametrisations. This has to be confronted with the earlier result from ZEUS[36] which suggested that the parametrisations of F_2^γ, obtained from fits to measurements made at e^+e^- colliders, are too low for medium values of Bjorken x and at factorisation scales of several hundred GeV^2. There are sev-

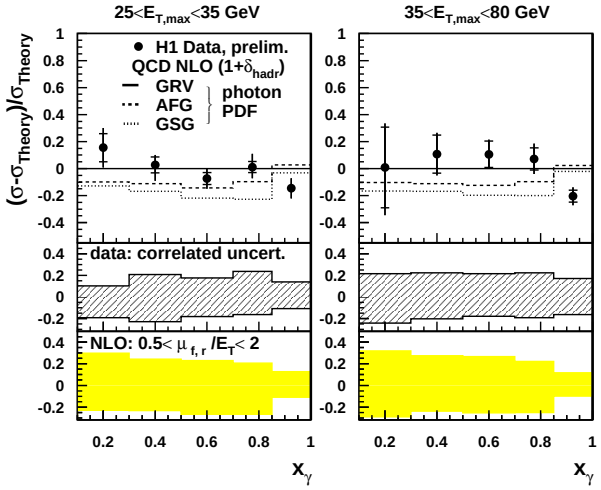

Figure 6. Measurement of the structure of quasi-real photons from H1.

eral differences between the ZEUS and H1 analysis such as the choice made for the value of α_s, the parton distributions used for the photon, and most notably the difference in the corrections applied to the data. The H1 data are corrected for detector as well as hadronisation effects and are shown at the partonic level. In contrast, the ZEUS results are corrected only for detector effects and phase space regions are selected, where the hadronisation corrections, as implemented in Monte Carlo models, are found to be small. It remains to be seen how much of the apparent differences between the results can be explained by the different analysis methods.

Also for the measurement of the structure of virtual photons some clarification is needed. The recent ZEUS measurement, Figure 7, indicates some shortcomings of the prediction from the SaS[37] parametrisations. The sup-

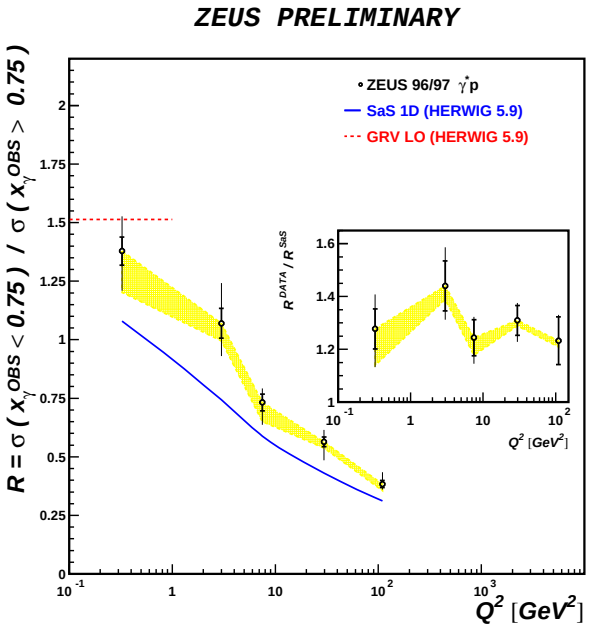

Figure 7. Measurement of the structure of virtual photons from ZEUS.

pression of the photon structure with the photon virtuality is studied based on the ratio of the cross sections for low and large values of x. The SaS1D prediction fails to describe this ratio. Again, there seems to be a difference between the ZEUS result and the earlier result from H1 on the structure of

virtual photons[38]. The H1 result, which is valid for an almost identical phase space region, showed good agreement between the data and the predictions based on the GRV parametrisation of F_2^γ with a virtuality suppression as given by the Drees-Godbole scheme.

It is certainly desirable to complement the measurements of F_2^γ with the jet measurements from HERA which extend to larger factorisation scales, when fits for the parton distribution functions of the photon are performed. However, first it has to be seen if a consistent picture of the various HERA results can be established.

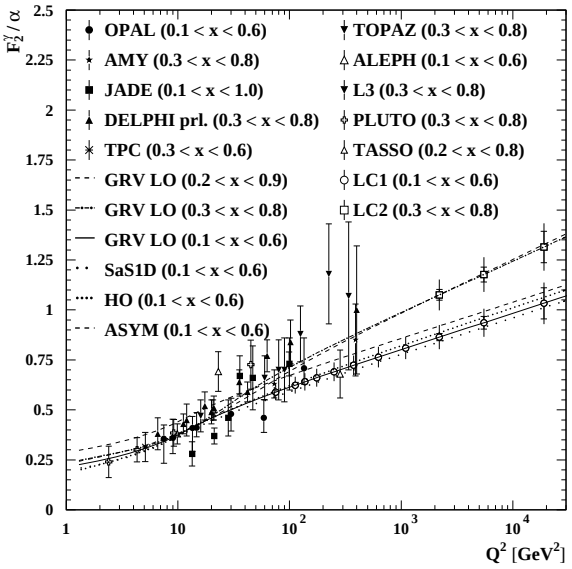

Figure 8. Prospects for the measurement of the F_2^γ at a future linear collider, from [33].

Recently at LEP progress has been made in the measurements of $F_2^\gamma(x, Q^2)$. The phase space of the measurement has been extended by OPAL[39], both to lower values of x and to larger values of Q^2. In addition, significant progress in reducing the systematic uncertainty has been achieved by using improved Monte Carlo models to describe the hadronic final state[40], as well as by utilising a more sophisticated unfolding procedure in two dimensions[41]. In view of these improvements a re-analysis of all LEP

data using the newly available analysis tools would significantly improve on the precision of F_2^γ.

The prospects of future investigations of the photon structure in the context of the planned linear collider programme are very promising[42]. The e^+e^- linear collider will extend the available phase space, as shown e.g. in Figure 8 for the measurement of the Q^2 evolution of F_2^γ at medium x. The higher beam energy and luminosity compared to LEP also allows for the investigation of novel features like the measurement of the flavour dependence of F_2^γ by exploring the exchange of Z and W bosons[43]. When using highly polarised beams the measurement of structure functions can be extended to polarised photons[44]. The investigation of the photon structure will enter a completely new level of sophistication if a photon collider can be realised[42]. Then photons of large energy with a rather moderate energy spread could be brought into collision, instead of the presently used soft photons from the Bremsstrahlungs spectrum at electron-positron colliders.

4 Proton structure

4.1 Deep inelastic scattering at high-Q^2

New measurements of the high-Q^2 neutral current (NC) and charged current (CC) deep inelastic scattering (DIS) $e^\pm p$ cross sections were presented by the ZEUS[45] and H1[46] collaborations [47]. Figure 9 shows the differential cross section $d\sigma/dQ^2$ for NC DIS. The ZEUS e^+p data, presented for the first time at this conference, were obtained using approximately 60 pb^{-1} of e^+p data collected at a centre-of-mass energy of $\sqrt{s} = 318$ GeV over the years 1999 and 2000. H1 has combined 46 pb^{-1} of e^+p data (from a total of 65 pb^{-1} collected in 1999 and 2000) at $\sqrt{s} = 318$ GeV with the 38 pb^{-1} of data collected over the years 1994 to 1997 at $\sqrt{s} = 300$ GeV. The NC cross section is observed to fall by roughly 6 orders of magnitude as Q^2 goes from $Q^2 \sim 200$ GeV^2 to $Q^2 \sim 10\,000$ GeV^2. For $Q^2 < 1\,000$ GeV^2 the NC e^+p cross section is observed to be approximately equal to the e^-p cross section. In this kinematic domain NC $e^\pm p$ DIS is mediated by single photon exchange and the Q^2 dependence of $d\sigma/dQ^2$ reflects the $1/Q^4$ dependence of the photon propagator. As Q^2 approaches the Z-boson mass squared ($Q^2 \sim M_Z^2$) the e^+p cross section falls below that for e^-p NC DIS. At such large Q^2 both photon- and Z-exchange contributions must be taken into account. The interference between the two contributions suppresses the e^+p cross section and enhances the e^-p cross section. The Standard Model (SM), which incorporates all these effects, evaluated with the CTEQ5[48] parton density functions (PDFs) gives a

good description of the data.

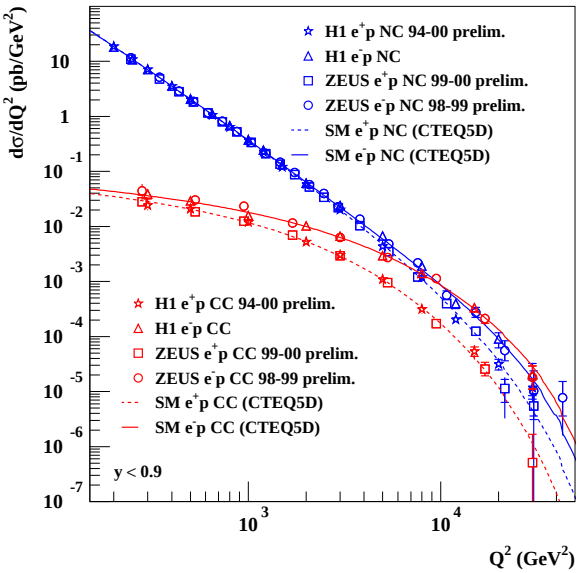

Figure 9. The high-Q^2 $e^{\pm}p$ neutral current and charged current deep inelastic scattering cross sections measured by the ZEUS and the H1 collaborations (points). The predictions of the Standard Model evaluated with the CTEQ5D parton density functions are shown as the lines.

The differential cross section $d\sigma/dQ^2$ for CC $e^{\pm}p$ DIS is shown in Figure 9. The cross sections fall slowly for $200 < Q^2 < 1\,000$ GeV^2 and then more rapidly as Q^2 approaches the W-boson mass squared ($Q^2 \sim M_W^2$). The SM, evaluated with the CTEQ5 PDFs, gives a good description of the data. The e^-p CC DIS cross section is always larger than the e^+p one. The CC interaction distinguishes between quarks of different flavour. Thus, the e^-p CC process picks out the up-type quarks and the down-type anti-quarks while e^+p CC DIS picks out the down-type quarks and the up-type anti-quarks. The e^-p cross section is larger than the e^+p cross section because there are more u-valence quarks than d-valence quarks in the proton and because the chiral nature of the CC interaction suppresses the contribution of the down-

type quarks in e^+p CC DIS. Note that for $Q^2 > 10\,000$ GeV^2 the four cross sections for NC and CC DIS in e^+p and e^-p collisions all have a similar magnitude. This is a striking experimental verification of the electroweak unification embodied in the Standard Model.

The reduced cross section $\tilde{\sigma}_{\rm NC}^{e^\pm p}$ is related to the double differential $e^\pm p$ NC DIS cross section by

$$Y_+\tilde{\sigma}_{\rm NC}^{e^\pm p} = \left[\frac{2\pi\alpha^2}{Q^4 x}\right]^{-1} \frac{d^2\sigma_{\rm NC}^{e^\pm p}}{dxdQ^2} = Y_+ F_2^{\rm NC} \mp Y_- xF_3^{\rm NC} - y^2 F_L^{\rm NC} \qquad (9)$$

where $Y_\pm = 1 \pm (1-y)^2$ and y is related to Q^2 and x by $Q^2 = xys$. Figure 10a shows $\tilde{\sigma}_{\rm NC}^{e^\pm p}$ plotted as a function of Q^2 for several values of x. For $Q^2 < 1\,000$ GeV^2 and $x \sim 0.1$ the reduced cross section is observed to be almost independent of Q^2 while for $Q^2 < 1\,000$ GeV^2 and $x > 0.25$ it falls slowly with Q^2. For Q^2 above $1\,000$ GeV^2 the e^-p reduced cross section exceeds the e^+p reduced cross section. The Standard Model (SM) expectations for $\tilde{\sigma}_{\rm NC}^{e^\pm p}$ obtained by evaluating Equation 9 using standard parton density functions gives a good description of the data. The SM accounts for the difference between $\tilde{\sigma}_{\rm NC}^{e^- p}$ and $\tilde{\sigma}_{\rm NC}^{e^+ p}$ in terms of the structure function $xF_3^{\rm NC}$ so that $xF_3^{\rm NC}$ may be extracted from the difference between $\tilde{\sigma}_{\rm NC}^{e^- p}$ and $\tilde{\sigma}_{\rm NC}^{e^+ p}$. Both ZEUS and H1 have extracted $xF_3^{\rm NC}$ in this way, the results are plotted in Figure 10b. A good description of the data is obtained when $xF_3^{\rm NC}$ is evaluated with standard PDFs. More e^-p data is required to improve the precision of $xF_3^{\rm NC}$. With sufficient data $xF_3^{\rm NC}$ will be used to constrain the valence quark PDFs.

The charged current can also be used to study the partonic content of the proton. The reduced cross section for $e^\pm p$ CC DIS, $\tilde{\sigma}_{\rm CC}^{e^\pm p}$, is defined to be

$$\tilde{\sigma}_{\rm CC}^{e^\pm p} = \left[\frac{G_F^2}{2\pi x}\frac{M_W^4}{\left(M_W^2+Q^2\right)^2}\right]^{-1} \frac{d^2\sigma_{\rm CC}^{e^\pm p}}{dxdQ^2} = \frac{1}{2}\left[Y_+ F_2^{\rm CC} \mp Y_- xF_3^{\rm CC} - y^2 F_L^{\rm CC}\right] \qquad (10)$$

Figure 11 shows $\tilde{\sigma}_{\rm CC}^{e^\pm p}$ as a function of x for values of Q^2 between 200 GeV^2 and $20\,000$ GeV^2. The SM expectation of Equation 10 gives a good description of the data. At leading order in QCD $\tilde{\sigma}_{\rm CC}^{e^+ p}$ is given by

$$\tilde{\sigma}_{\rm CC}^{e^+ p} = x\left[\bar{u} + \bar{c} + (1-y)^2(d+s)\right] \qquad (11)$$

while $\tilde{\sigma}_{\rm CC}^{e^- p}$ is given by

$$\tilde{\sigma}_{\rm CC}^{e^+ p} = x\left[u + c + (1-y)^2(\bar{d}+\bar{s})\right] \qquad (12)$$

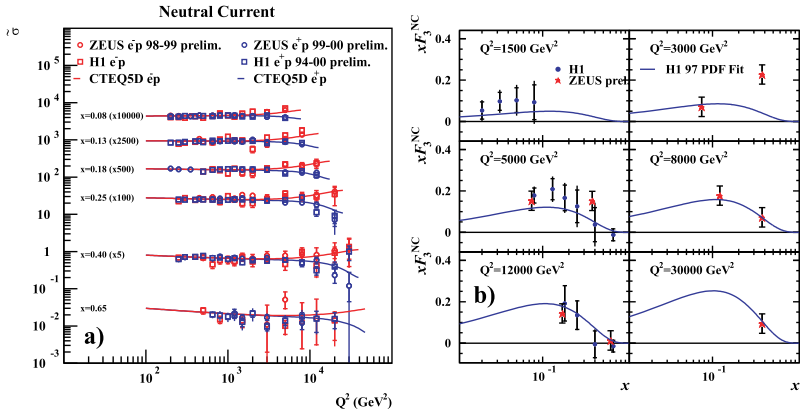

Figure 10. (a) The reduced cross section for $e^{\pm}p$ neutral current deep inelastic scattering measured by the ZEUS and the H1 collaborations (points). The predictions of the Standard Model evaluated with the CTEQ5D parton density functions are shown as the lines. (b) The neutral current structure function $xF_3^{\rm NC}$ extracted from $e^{\pm}p$ neutral current deep inelastic scattering data by the ZEUS and H1 collaborations (points). The predictions of the Standard Model evaluated with the CTEQ5D parton density functions are shown as the solid lines.

Figure 11 shows how the different quark flavours contribute to the reduced cross section. It can be seen that, at high-x, $\tilde{\sigma}_{\rm CC}^{e^+p}$ is sensitive to the d-quark density while $\tilde{\sigma}_{\rm CC}^{e^-p}$ is sensitive to the u-quark density.

These results, important in themselves, represent a significant milestone in the development of the HERA physics programme. DIS01 took place at a time when major upgrades to the HERA machine and experiments were nearing completion[49,50]. The HERA machine upgrade will provide polarised electron and positron beams for the colliding beam experiments ZEUS and H1 at a luminosity five times greater than has been achieved to date. The new high-Q^2 cross section results, therefore, represent the culmination of the programme of measurements of the unpolarised DIS cross sections at high-Q^2.

4.2 Determination of $\alpha_{\rm S}$ and extraction of the gluon density

A highlight of the structure function session was the variety of new, high precision, simultaneous determinations of the strong coupling constant, $\alpha_{\rm S}$, and the gluon density, xG. The ZEUS[51] and H1[52] collaborations presented new analyses in which the scaling violations of the structure function $F_2^{\rm NC}$

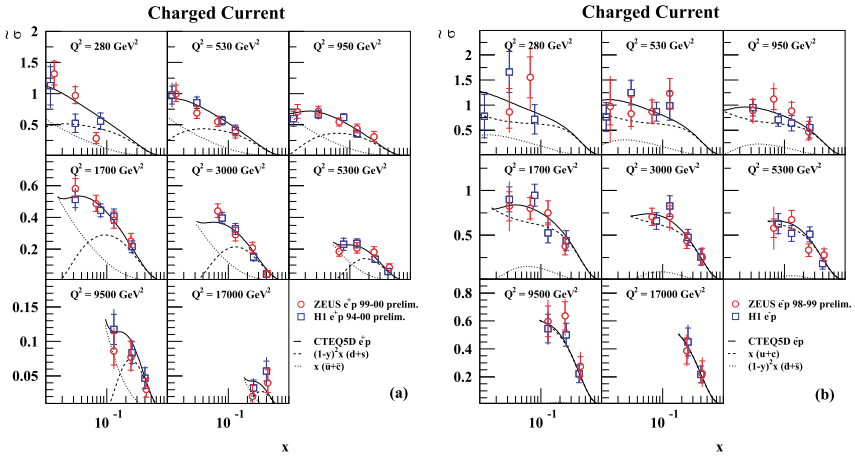

Figure 11. The reduced cross section for e^+p (a) and e^-p (b) charged current deep inelastic scattering measured by the ZEUS and the H1 collaborations (points). The predictions of the Standard Model evaluated with the CTEQ5D parton density functions are shown as the solid lines. Quark contributions, evaluated using the CTEQ5D PDFs, are shown as the dashed lines.

are exploited to determine xG and α_S. Both collaborations have performed a NLO QCD fit using their own data on $\tilde{\sigma}^{e^+p}_{NC}$ together with structure function data from other experiments. The analyses proceed by parameterising the PDFs at a starting scale Q_0^2. The DGLAP equations[53] are used to evolve from Q_0^2 to the value of Q^2 that corresponds to a particular data point. The relevant measured quantity is then determined from the evolved PDFs and the contribution to the total χ^2 calculated. The ZEUS and H1 analyses differ both in philosophy and in the details of the fitting technique used.

The goal of the H1 collaboration was to determine xG and α_S as precisely as possible using as few data sets as possible. The fit includes data from H1[54] and BCDMS[55] (proton target data) in order that the lever arm in x and Q^2 be sufficient to constrain the parameterisation. The PDFs are parameterised at $Q_0^2 = 4$ GeV^2. The PDF parameterisation is based on effective valence and sea distributions together with a parameterisation for xG. The number of parameters in the gluon and sea distributions are chosen to saturate the χ^2. The c- and b-quark contributions to the cross sections are evaluated using photon-gluon fusion using a massive fixed flavour number scheme[56].

ZEUS parameterised the u- and d-valence, the sea and the gluon PDFs at

$Q_0^2 = 7$ GeV^2. In addition, the difference between the u- and d-quark density ($x(u-d)$) was parameterised. The recent ZEUS data[57] was used together with data from BCDMS[55], CCFR[58], NMC[59] and E665[60]. A modified massive variable flavour number scheme (RT-VFN scheme[61]) was used. This treatment of the charm quark smoothly interpolates between the low-Q^2 region where threshold effects are important to the high-Q^2 region where the charm quark mass is negligible.

Both ZEUS and H1 have incorporated a very careful treatment of the experimental systematic errors which includes the point-to-point correlations. H1 allowed the fit to determine the best values for the various systematic uncertainties, the ZEUS fit did not. The resulting gluon distributions are compared in Figure 12a. When the differences between the two analyses are taken into account the agreement between the two results is reasonable. The corresponding values of α_S are

$$\alpha_S = 0.1172 \pm 0.0008(\text{stat.} + \text{uncor. sys.}) \pm 0.0054(\text{cor.sys.}) \quad \text{(ZEUS)} \quad (13)$$

$$\alpha_S = 0.1150 \pm 0.0017(\text{expt.})^{+0.0009}_{-0.0005}(\text{model}) \pm 0.005(\text{scale}) \quad \text{(H1)} \quad (14)$$

ZEUS breaks up the total experimental uncertainty into the contribution arising from the correlated experimental systematic uncertainties (cor. sys.) and the combined statistical and uncorrelated systematic uncertainties (stat. + uncor. sys.). H1 has combined the statistical and experimental systematic contributions into a single error labeled (expt.). The H1 'model' error accounts for uncertainties in the theoretical model such as those arising from the choice of the functional form or the treatment of heavy quarks while the 'scale' error is evaluated by varying the factorisation and renormalisation scales. The values obtained are consistent with one another and with the values obtained in various global analyses[62]. Given the importance of the measurements it will be important to understand in detail the range of applicability of the results and, if possible, to converge upon a common approach.

The ZEUS[63] and H1[64] collaborations have exploited the sensitivity of DIS jet production cross sections to determine α_S and xG. With α_S set equal to the world average, xG may be determined in a fit to the measured inclusive jet cross sections. This has been done by H1 and the result is shown in Figure 12b[66]. Alternatively, the PDFs can be taken from one of the standard parameterisations and the jet cross sections used to determine α_S. When α_S is determined in this way it is essential to estimate the uncertainty in α_S which arises from the choice of PDF. Both ZEUS[65] and H1[66] have performed such analyses. The H1 analysis uses the inclusive jet cross section. ZEUS has chosen to analyse the ratio of the cross section for the production of 2-jets (plus the target remnant) to the total inclusive DIS cross section. The

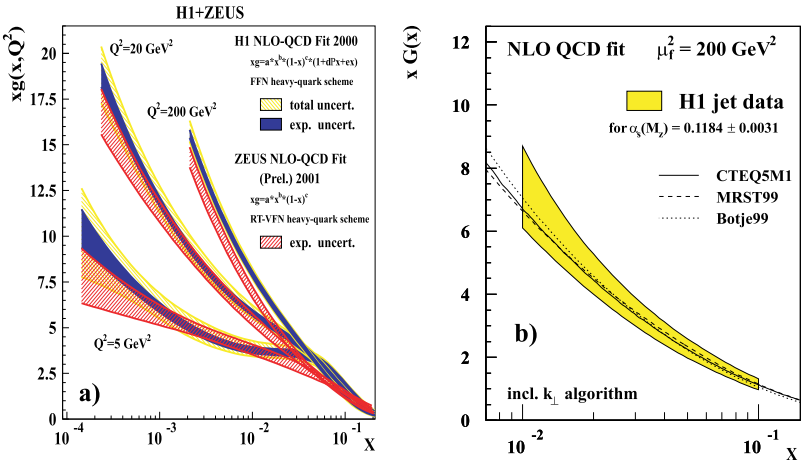

Figure 12. (a) The gluon distributions extracted from the ZEUS and H1 NLO QCD fits to structure function data. The statistical and systematic error bands are shown shaded. Details of the extraction of these error bands may be found elsewhere in these proceedings. (b) The gluon distribution extracted from a NLO QCD fit to the H1 inclusive jet cross section data.

use of the ratio reduces the sensitivity of the result to the choice of PDF. A compilation of the values of α_S obtained from jet production data is shown in Figure 13 together with the results obtained from the scaling violations of F_2. The results agree with one another and with the world average. The way in which α_S depends on Q^2, the running of α_S, may also be investigated using the jet data. Both ZEUS[65] and H1[66] have performed such analyses and the results are consistent with the QCD expectation. Finally, it is also possible to estimate xG and α_S simultaneously from the jet data in a fit conceptually similar to that used in the analysis of the scaling violations of F_2^{NC} described above. The H1[66] collaboration has performed such an analysis. The fit results in estimates of the gluon distribution and α_S which are correlated.

The techniques discussed above do not constrain the gluon distribution for $x > 0.1$. A promising new development is the measurement of the double differential inclusive jet cross section $d^2\sigma/dE_T d\eta$ (where E_T is the jet transverse energy and η is the jet pseudo-rapidity) by the D0 collaboration[67,68]. The cross sections, shown in Figure 14, have been measured over the kinematic range $|\eta| < 3$ and $50 < E_T < 500$ GeV. Since the beam energy at the Tevatron is 900 GeV, these cross sections are sensitive to xG for values of x as high as

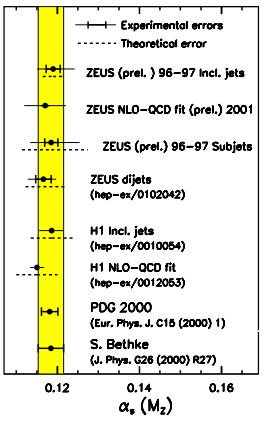

Figure 13. Compilation of the various determinations of the strong coupling constant, α_S, at HERA together the results of two global analyses.

$x \sim 0.9$. The sensitivity of these cross sections to the gluon was demonstrated by evaluating a χ^2 formed between the measurements and the inclusive jet cross section evaluated using various standard PDF sets. The χ^2 evaluation took account of correlations between uncertainties in the variables η and E_T. The results indicate that the data prefer a slightly harder gluon distribution than is contained within the standard CTEQ4[69] parameterisation. NLO QCD fits incorporating the D0 inclusive jet data are being prepared by the MRST and the CTEQ groups. The data will provide a stringent constraint on the gluon density at high-x.

4.3 Structure functions at low-Q^2

It is well established that $F_2^{\rm NC}$ rises rapidly as x falls below $x \sim 0.01$ so long as Q^2 is larger than ~ 2 GeV^2 and that NLO QCD gives a good description of the data for $Q^2 > 2$ GeV^2 [54,57]. Precise measurements of $F_2^{\rm NC}$ for Q^2 in the range $0.045 < Q^2 < 0.65$ GeV^2 show that in this kinematic domain $F_2^{\rm NC}$ does not rise rapidly as x falls[70]. The low Q^2 data can be described using non-perturbative models. The x dependence of $F_2^{\rm NC}$ appears to undergo a transition at a Q^2 of around 1 GeV^2. The nature of the transition between

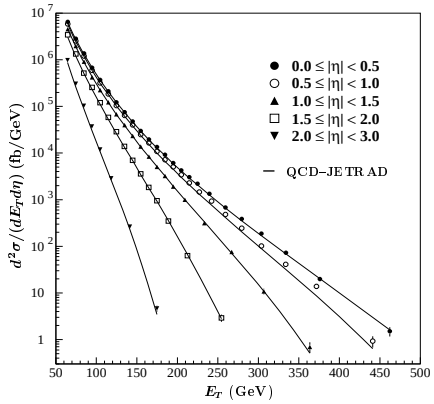

Figure 14. Inclusive double differential single inclusive jet cross sections measured by the D0 collaboration (points) for jet pseudo-rapidity (η) intervals plotted as a function of the jet transverse energy (E_T). The Standard Model prediction is shown as the solid line.

the kinematic domain where perturbative QCD is applicable and the domain where non-perturbative strong interaction physics is important was discussed in a dedicated session at this workshop. The contributions to this session are summarised elsewhere in these proceedings[71]. A new measurement of $F_2^{\rm NC}$ spanning the Q^2 range $0.35 < Q^2 < 20$ GeV^2 was presented by the H1 collaboration[72]. The low values of Q^2 were accessed by selecting a sample of events in which a photon was radiated in the direction of the incoming positron. Such initial state radiation (ISR) causes the effective centre-of-mass energy in the e^+p collision to be reduced. Hence, a scattered positron of particular energy and scattered through a particular angle results from a DIS collision is characterised by a smaller value of Q^2 and a higher value of x than would be the case if a scattered positron with the same energy and scattering angle were found in the absence of ISR. Figure 15 shows the resulting F_2 plotted as a function of Q^2 at several values of W, the centre-of-mass energy in the virtual photon-proton system. The new H1 ISR measurement spans the transition region around $Q^2 \sim 1$ GeV^2. Further measurements in this important kinematic region will be required in order that an understanding of the underlying physics may be developed.

The CCFR collaboration has resolved the long-standing discrepancy between the structure functions extracted from neutrino-nucleon CC DIS and those extracted from muon-nucleon NC DIS[73,74]. The expression for the cross sections for CC νN DIS contains three structure functions, just as Equation

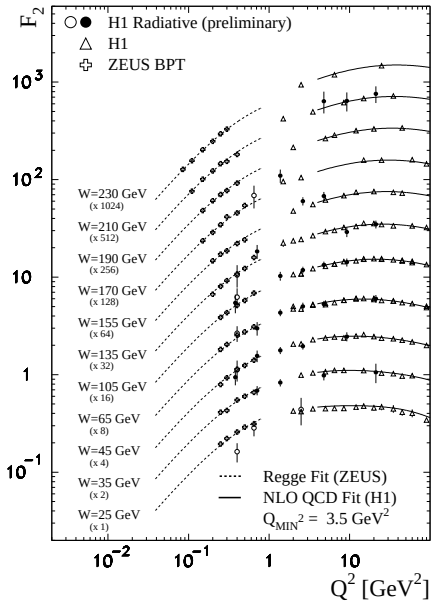

Figure 15. Compilation of ZEUS and H1 measurements of F_2 at low-Q^2 in NC DIS (points) plotted at several values of W as a function of Q^2. The solid lines show the result of the H1 NLO QCD fit to the H1 F_2 data for $Q^2 > 3.5$ GeV^2. The dashed lines show the result of the ZEUS Regge fit to the ZEUS F_2 data for $Q^2 < 0.65$ GeV^2.

10 does, but the quark composition of these structure functions in the Quark Parton Model differs from those given in Equations 11 and 12[75]. The CCFR data were re-analysed[73,74] taking charm mass effects into account when evaluating NLO QCD corrections for the longitudinal structure function and the difference between the structure function xF_3 for νN and $\bar{\nu} N$ CC DIS. In addition to an update of the structure function F_2^ν for $Q^2 > 1$ GeV^2, the CCFR collaboration presented results on F_2^ν for $Q^2 < 1$ GeV^2 [73,76]. This is the first time that F_2^ν has been determined for such low values of Q^2.

4.4 The longitudinal structure function, $F_{\rm L}^{\rm NC}$

The structure function $F_{\rm L}^{\rm NC}$ is multiplied by a factor of y^2 in the expression for the cross section for NC e^+p DIS. This makes $F_{\rm L}^{\rm NC}$ difficult to determine at HERA since the NC cross section $d^2\sigma_{\rm NC}^{e^+p}/dxdy \propto 1/y^2$ at fixed x. A direct determination of $F_{\rm L}^{\rm NC}$ can be made by reducing the proton beam energy and so

raising the value of y for fixed x and Q^2 [77]. The difference between the proton beam energies at which HERA has operated to date (820 GeV and 920 GeV) is too small to allow an extraction of $F_{\rm L}^{\rm NC}$. H1 has developed two methods of extracting $F_{\rm L}^{\rm NC}$ [54]. In the first, indirect, method a NLO QCD fit was made to the reduced cross section for $y < 0.3$ where the contribution of $F_{\rm L}^{\rm NC}$ may be neglected. This fit was then extrapolated to larger values of y and the difference between the extrapolation and the data taken as a measure of $F_{\rm L}^{\rm NC}$. For Q^2 less than 10 GeV^2 $d\sigma_{\rm NC}^{e^+p}/d\ln y$ was used instead of the NLO QCD fit to extrapolate to high-y[78]. Secondly, the ISR technique, outlined above, has been used to vary the effective centre-of-mass energy so that $F_{\rm L}^{\rm NC}$ can be extracted. Both methods rely upon the measurement of the reduced cross section at the highest possible y. At DIS01 the H1 collaboration presented new data on $\tilde{\sigma}^{e^+p}$ for $1.5 < Q^2 < 12$ GeV^2 from a sample that contains scattered positrons with energies as low as 3 GeV. As a result y values as high as 0.9 can be accessed. In addition, H1 has extracted $F_{\rm L}^{\rm NC}$ for Q^2 values as high as 700 GeV^2 [46]. Figure 16 shows the values of $F_{\rm L}^{\rm NC}$ extracted using these methods as well as the $F_{\rm L}^{\rm NC}$ resulting from the fit to the F_2 data for $y < 0.3$.

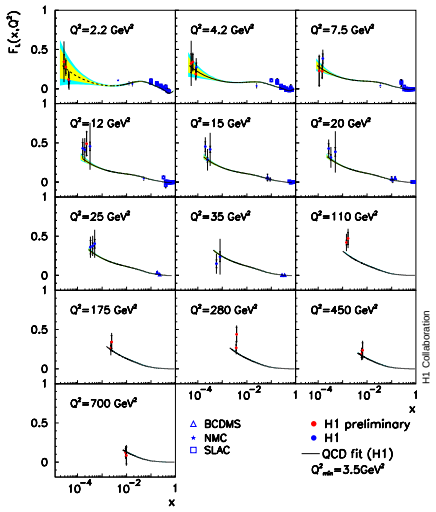

Figure 16. The longitudinal structure function, F_L, extracted from NC ep DIS data by the H1 collaboration.

The structure function R^ν ($F_{\rm L}^\nu \approx [R^\nu/(1+R^\nu)]\,F_2^\nu$) extracted from νN and $\bar{\nu}N$ data by the CCFR collaboration has been measured[79]. R^ν was pre-

sented over the kinematic range $0.004 < x < 0.5$ and $0.5 < Q^2 < 200$ GeV^2. The data are well described by NLO QCD evaluated using the MRST PDFs[80].

4.5 Flavour specific parton density functions

Much can be inferred about the partonic structure of the proton from the inclusive measurements discussed above. A deeper understanding can be developed using measurements of the cross sections for processes that are sensitive to specific quark flavours. The sensitivity of CC data from HERA to the d- and u-quark densities was discussed in Section 4.1. An estimate of the PDF ratio $\bar{d}/\bar{u}$ can be obtained by determining the cross section for the Drell-Yan processes $pN \rightarrow \mu^+\mu^- X$ where N is either a proton or a deuteron. Final measurements of the proton-proton to proton-deuteron Drell-Yan cross section ratio from the E866 experiment at Fermilab were presented[81]. The Bjorken-x of the two partons that annihilate, x_1 and x_2, can be reconstructed from the combined four momentum of the muon pair. When $x_1 >> x_2$ the cross section ratio is approximately given by

$$\frac{\left.\frac{d^2\sigma^{pd}}{dx_1 dx_2}\right|_{x_1>>x_2}}{\left.\frac{d^2\sigma^{pp}}{dx_1 dx_2}\right|_{x_1>>x_2}} \approx \left[1 + \frac{\bar{d}(x)}{\bar{u}(x)}\right] \tag{15}$$

where $x = x_2$. The $\bar{d}/\bar{u}$ ratio extracted from Equation 15 by the E866 collaboration is observed to peak at $x \sim 0.18$[81]. This measurement will give an important constraint on the sea quark density at intermediate to high-x.

Charm production in DIS at HERA has been exploited by both the ZEUS[82] and the H1[83] collaborations to extract $F_2^{c\bar{c}}$, the charm contribution to $F_2^{\rm NC}$. To date two methods have been used to tag charm in DIS. The first method, used by ZEUS and H1, exploits the small mass difference between the charmed mesons in the decay $D^* \rightarrow D^0\pi$ to identify D^* production. The ZEUS collaboration has also used the electrons produced in semi-leptonic charm decays. The selection of the semi-leptonic sample was challenging and was performed by combining information on the electromagnetic shower profile in the calorimeter with the energy loss information obtained from the central drift chamber. The steps by which $F_2^{c\bar{c}}$ was extracted are common to both collaborations. First the DIS charm cross section times branching ratio was measured in a region of phase space limited by the acceptance of the apparatus. Next, the cross section was extrapolated to the full phase space using QCD based Monte Carlo programs and the known branching ratios of the charmed hadrons taken into account. Finally, $F_2^{c\bar{c}}$ was extracted from the charm production cross section. The results are plotted in Figure 17. $F_2^{c\bar{c}}$

is observed to rise rapidly as x falls, a behaviour that mirrors the behaviour of the inclusive $F_2^{\rm NC}$. In addition, $F_2^{c\bar{c}}$ is observed to exhibit the strong scaling violations expected in NLO QCD calculations of $F_2^{c\bar{c}}$ based on standard PDFs. $F_2^{c\bar{c}}$ is large, amounting to $\sim 25\%$ of $F_2^{\rm NC}$ for $Q^2 \sim 30$ GeV^2 and $x \sim 10^{-3}$. The high luminosity that will be provided by the HERA upgrade coupled with the increased charm sensitivity offered by the new ZEUS and H1 silicon micro-vertex detectors promises rapid progress in this field.

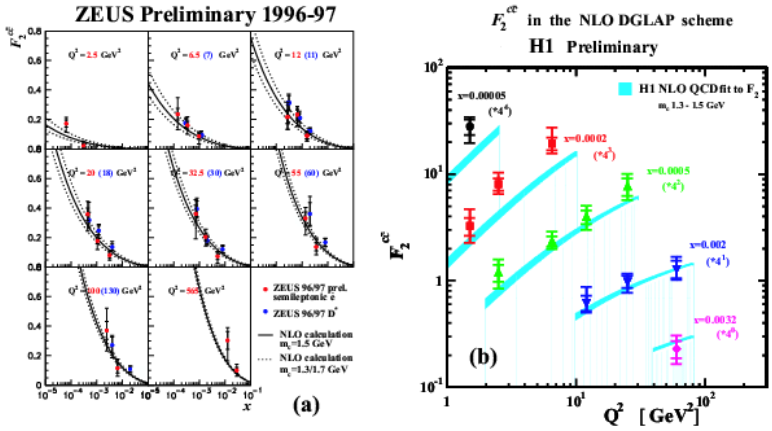

Figure 17. The charm contribution to $F_2^{\rm NC}$, $F_2^{c\bar{c}}$. (a) $F_2^{c\bar{c}}$ plotted as a function of x for several values of Q^2 (points). The solid line shows the result of a NLO QCD calculation. (b) $F_2^{c\bar{c}}$ plotted as a function of Q^2 for several values of x. The expectations of the H1 NLO QCD fit are shown as the shaded bands.

The CCFR and the NuTeV collaborations each presented several new results that are sensitive to the flavour content of the proton. NuTeV[84] presented final cross sections for dimuon production in νN and $\bar{\nu} N$ DIS. Dimuon production in CC νN DIS is sensitive to the strange quark density. By making a NLO QCD fit to the νN and the $\bar{\nu} N$ dimuon data NuTeV has been able to demonstrate that the magnitude of the strange sea amounts to approximately 40% of the up-quark sea and that the s-quark density has approximately the same magnitude as the $\bar{s}$-quark density. Samples of NC νN and $\bar{\nu} N$ events containing a low energy muon were also studied. The muons in these events arise from the decay of hadrons produced in the scattering. Single muon production in NC νN and $\bar{\nu} N$ DIS is sensitive to the charm quark density. The NuTeV results do not require the introduction of intrinsic charm. CCFR[79] has determined the difference between the structure function $xF_3^{\bar{\nu}}$ in CC $\bar{\nu} N$

scattering and the structure function xF_3^ν in CC νN scattering, $\Delta(xF_3^\nu)$. In the quark parton model $\Delta(xF_3^\nu) = 4x(s-c)$. $\Delta(xF_3^\nu)$ was presented in the kinematic range $0.015 < x < 0.08$ and for $7 < Q^2 < 20$ GeV^2. The data are reasonably well described by NLO QCD using standard PDF sets.

4.6 The future of lepton-nucleon deep inelastic scattering

The upgrade to the HERA accelerator, which was nearing completion at the time DIS01 was held, will yield a factor five more luminosity and deliver polarised electron and positron beams to the collider experiment ZEUS and H1. The ZEUS and H1 experiments are also undergoing far reaching upgrades. The upgrades themselves and the physics opportunities of the new machine and detectors are described elsewhere in these proceedings [49,50]. Looking further ahead there are two new windows on lepton-nucleon deep inelastic scattering that were discussed at DIS01. The first, *ep* collisions between 920 GeV protons from the HERA proton ring and 250 GeV electrons or positrons from the proposed TESLA linac, offers exciting possibilities in the study of low-x DIS and diffraction[85]. The second, νN scattering, would use the intense neutrino beam generated by the decay in flight of the intense stored muon beam of a future Neutrino Factory[86]. The unprecedented neutrino flux that such a facility will provide will allow neutrino targets with a mass of only a few kilogrammes to be used. Not only would experiments at such a facility be able to determine all the unpolarised neutrino-nucleon structure functions with great precision but the flux would be high enough that high precision measurements using polarised nuclear targets will be possible.

Acknowledgments

We very much enjoyed this well organised workshop in the beautiful town of Bologna, and we thank the organisers for the support and hospitality given to us. We would also like to thank all those who contributed to the structure function session either by preparing talks or by taking part in the lively debates. We greatly appreciate the help that we have been given by the speakers in preparing the summary talks and in the preparation of these proceedings.

References

1. A. Retey and J.A.M. Vermaseren, *Nucl. Phys.* **B604**, 28 (2001).
2. W.L. van Neerven and A. Vogt, *Nucl. Phys.* **B568**, 263 (2000); **B588**, 345 (2000); *Phys. Lett.* **B490**, 111 (2000).

3. A. Vogt, these proceedings.
4. J. Blümlein, these proceedings.
5. J. Blümlein, V. Ravindran, Jian-hong Ruan and Wei Zhu, *Phys. Lett.* **B504**, 235 (2001).
6. L. Magnea, these proceedings.
7. L. Magnea, *Nucl. Phys.* **B593**, 269 (2001).
8. A.V. Kotikov and G. Parente, these proceedings and references therein.
9. A. De Rújula *et al.*, *Phys. Rev.* **D10**, 1649 (1974);
   R.D. Ball and S. Forte, *Phys. Lett.* **B336**, 77 (1994);
   L. Mankiewicz, A. Saalfeld and T. Weigl, *Phys. Lett.* **B393**, 175 (1997).
10. M. Beneke and V.M. Braun, preprint hep-ph/0010288 (2001).
11. B.I. Ermolaev, these proceedings.
12. B.I. Ermolaev, M. Greco and S.I. Troyan, *Nucl. Phys.* **B571**, 2137 (2000); **B594**, 71 (2001).
13. A. Szczurek, these proceedings.
14. A. Szczurek, N.N. Nikolaev, W. Schäfer and J. Speth, *Phys. Lett.* **B500**, 254 (2001).
15. I.P. Ivanov and N.N. Nikolaev, preprint hep-ph/0004206 (2000).
16. A.D. Martin, R.G. Roberts, W.J. Stirling and R.S. Thorne, these proceedings.
17. A.D. Martin, R.G. Roberts, W.J. Stirling and R.S. Thorne, *Eur. Phys. J.* **C14**, 133 (2000).
18. D. Stump *et al.*, preprint hep-ph/0101051 (2001).
19. W.T. Giele, S.A. Keller, preprint hep-ph/0104053 (2001).
20. M. Botje, *Eur. Phys. J.* **C14**, 285 (2000).
21. S. Alekhin, *Phys. Rev.* **D63**, 094022 (2001); *Eur. Phys. J.* **C10**, 395 (1999).
22. J. Pumplin *et al.*, preprint hep-ph/0101032 (2001).
23. V. Barone, C. Pascaud and F. Zomer, *Eur. Phys. J.* **C12**, 243 (2000).
24. W.T. Giele, S.A. Keller and D.A. Kosower, preprint hep-ph/0104052 (2001).
25. D. Stump, these proceedings and references therein.
26. J.C. Collins and J. Pumplin, these proceedings.
27. J.C. Collins and J. Pumplin, preprint hep-ph/0105207 (2001).
28. S. Kumano, these proceedings.
29. M. Hirai, S. Kumano and M. Miyama, *Phys. Rev.* **D64**, 034003 (2001).
30. K.J. Eskola, V.J. Kolhinen and P.V. Ruuskanen, *Nucl. Phys.* **B535**, 351 (1998).
31. K.J. Eskola, V.J. Kolhinen, C.A. Salgado and R.L. Thews, preprint hep-ph/0009251 (2000).

32. K.J. Eskola, V.J. Kolhinen and R. Vogt, preprint hep-ph/0104124 (2001).
33. R. Nisius, *Phys. Rep.* **332**, 165 (2000).
34. S. Ferron, these proceedings.
35. D. Kcira, these proceedings.
36. ZEUS Collaboration, J. Breitweg *et al.*, *Eur. Phys. J.* **C11**, 35 (1999).
37. G.A. Schuler and T. Sjöstrand, Z. Phys. **C68**, 607 (1995).
38. H1 Collaboration, C. Adloff *et al.*, *Eur. Phys. J.* **C13**, 397 (1999).
39. R. Taylor, these proceedings.
40. The LEP Working Group for Two-Photon Physics, ALEPH, L3, and OPAL Collaborations, CERN-EP-2000-109, preprint hep-ex/0010041 (2001).
41. OPAL Collaboration, G. Abbiendi *et al.*, *Eur. Phys. J.* **C18**, 15 (2000).
42. A. De Roeck, these proceedings;
    TESLA, Technical Design Report, Part III, preprint hep-ph/0106315.
43. A. Gehrmann-De Ridder et. al, *Phys. Lett.* **B469**, 259 (1999).
44. M. Stratmann, *Nucl. Phys. B (Proc. Suppl.)* **82**, 400 (2000).
45. A. Lopez Duran Viani, these proceedings and references therein.
46. A. Dubak, these proceedings and references therein.
47. ZEUS Collaboration, J. Breitweg *et al.*, Eur. Phys. J. **C11** 427 (1999);
    H1 Collaboration, C. Adloff *et al.*, Eur. Phys. J. **C13** 609 (2000);
    H1 Collaboration, C. Adloff *et al.*, DESY 00-187 (2000).
48. CTEQ Collaboration, H.L. Lai *et al.*, Eur. Phys. J. **C12** 375 (2000).
49. E. Elsen, these proceedings and references therein.
50. B. Foster, these proceedings and references therein.
51. K. Nagano, these proceedings and references therein.
52. R. Wallny, these proceedings and references therein.
53. G. Parisi, Proc 11th Recontre de Moriond (1976);
    G. Altarelli & G. Parisi, Nucl. Phys. **B126** 298 (1977);
    V. Gribov & L. Lipatov, Sov. Jour. Nucl. Phys. **15** 438 (1972);
    L. Lipatov, Sov. Jour. Nucl. Phys. **20** 94 (1975);
    Y. Dokshitzer, Sov. Phys. JETP **46** 641 (1977).
54. H1 Collab., C. Adloff *et al.*, DESY-00-181 (2000)
55. BCDMS Collaboration, A.C. Benvenuti *et al.*, Phys. Lett. **B223** 485 (1989);
    CERN preprint CERN-EP/89-06.
56. E. Laenen *et al.*, Nucl. Phys. **B79** Proc. Suppl. (1992), ed. by J. Blümlein and T. Reimann; hep-ph/9906337.
57. ZEUS Collaboration, J. Breitweg *et al.*, DESY-01-064, submitted to Eur. Phys. J.
58. CCFR Collaboration, W.G. Seligman *et al.*, Phys. Rev. Lett. **79** 1213

(1997).
59. NMC Collaboration, M. Arneodo *et al.*, Nucl. Phys. **B483** 3 (1997); NMC Collaboration, M. Arneodo *et al.*, Nucl. Phys. **B487** 3 (1997).
60. E665 Collaboration, M.R.Adams *et al.*, Phys. Rev. **D54** 3006 (1996).
61. R.G. Roberts and R.S. Thorne, J. Phys. **G25** 1307 (1999); R.G. Roberts and R.S. Thorne, Phys. Lett. **B421** 303 (1998); R.G. Roberts and R.S. Thorne, Phys. Rev. **D57** 6871 (1998); R.G. Roberts and R.S. Thorne, Eur. Phys. **C19** 339 (2001).
62. Particle Data Group, D.E. Groom *et al.*, Review of particle physics, Eur. Phys. J. **C15** 1 (2000); S. Bethke, J. Phys. **G26** R 27 (2000).
63. E. Tassi, these proceedings and references therein.
64. G. Grindhammer, these proceedings and references therein.
65. ZEUS Collaboration, J. Breitweg *et al.*, Phys. Lett. **B507** 70 (2001).
66. H1 Collaboration, C. Adloff *et al.*, Eur. Phys. J. **C19** 289-311 (2001).
67. L. Babukhadia, these proceedings and references therein.
68. D0 Collaboration, B. Abbot *et al.*, Phys. Rev. Lett. **86** 1707 (2001).
69. CTEQ Collaboration, H.L. Lai *et al.*, Phys. Rev. **D51** 4763 (1995).
70. ZEUS Collaboration, J. Breitweg *et al.*, Phys. Lett. **B487** 53 (2000).
71. J. Bartels, these proceedings and references therein.
72. C. Issever, these proceedings and references therein.
73. R. Bernstein, these proceedings and references therein.
74. CCFR Collaboration, U.K. Yang *et al.*, accepted by Phys. Rev. Lett.
75. See for example A.M. Cooper-Sarkar, R.C.E. Devenish, A. De Roeck, Int. J. Mod. Phys. **A13** 3385 (1998).
76. CCFR Collaboration, B.T. Fleming *et al.*, hep-ex/0011094 accepted by Phys. Rev. Lett.
77. See for example A.M. Cooper-Sarkar *et al.*, Z. Phys. **C39** 281 (1988).
78. D. Eckstein, these proceedings and references therein.
79. A. Bodek, these proceedings and references therein.
80. A.D.Martin et al, A.D. Martin, R.G. Roberts, W.J. Stirling, R.S. Thorne, Nucl. Phys. Proc. Suppl. **79** 105 (1999); A.D. Martin, R.G. Roberts, W.J. Stirling, R.S. Thorne, Eur. Phys. J. **C4** 463 (1998).
81. D. Isenhower, these proceedings and references therein.
82. S. Schagen, these proceedings and references therein.
83. S. Mohrdieck, these proceedings and references therein.
84. M. Goncharov, these proceedings and references therein.
85. M. Klein, these proceedings and references therein.
86. J.G. Morfin, these proceedings and references therein.